Performance of Reed-Muller Codes with OFDM and a Maximum Likelihood Decoding Algorithm

Alan E. Jones, Tim A. Wilkinson
Appliance Communications Solutions Department
HP Laboratories Bristol
HPL-98-88
April, 1998

E-mail: [aj,taw]@hplb.hpl.hp.com

OFDM,
Reed-Muller,
ACI,
Golay
complementary
sequences

The performance of OFDM with Reed-Muller encoding and a maximum likelihood decoding algorithm is presented. The example codes are shown to have a tightly bounded peak-to-mean envelope power ratio of at most 3.0dB, whilst simultaneously enabling good error correction. Using both experimental and simulated results the codes are shown to offer superior adjacent channel interference performance when compared to an OFDM system that exhibits the same peak-to-mean envelope power ratio as an uncoded system. We present a maximum likelihood decoder which makes use of a distance preserving map and multiple fast Hadamard transforms. Its operation is described in detail and its performance is assessed using a number of realistic channel conditions.

Internal Accession Date Only

© Copyright Hewlett-Packard Company 1998

1 Introduction

Multicarrier modulation or OFDM (orthogonal frequency division multiplexing) [1,2] has been proposed or adopted for many different types of radio systems from wireless LANs [3] to digital audio and video broadcasting [4]. The essence of the technique is parallel transmission of data on multiple carriers using Fourier transform processing for modulation and demodulation. Its advantageous properties are well known and extensively documented. It has inherent resistance to dispersion in the propagation channel and, with the addition of coding, frequency diversity can be exploited in frequency selective fading channels giving excellent performance in low signal to noise conditions [5,6]. Thus in many instances OFDM is often preferred to the alternative of adaptive equalisation. It is also arguably less complex for the same transmission rate capability [7]. However OFDM does have its disadvantages. One of the most obvious disadvantages is that an OFDM signal has a non-constant envelope and thus requires linear transmit and receive chains in a system for faithful transmission of a signal. More specifically, as the OFDM signal consists of multiple modulated carriers the envelope distribution is Gaussian with peaks which are much higher than the mean when these add constructively.

This problem manifests itself in a number of different ways depending on how the system designer is constrained. If there is a peak power limit in the band then the mean power permissible using OFDM will be less than that with a constant envelope modulation scheme. However this reduction in power must be offset against the performance advantage OFDM might have against a solution with constant envelope modulation and adaptive equalisation. Quite often portable equipment design is constrained by battery power. As OFDM requires linear amplification this inevitably means operating power amplifiers with considerable back-off from compression and with the associated reduction in efficiency. In either case there is an obvious need to limit the envelope fluctuation of a multicarrier signal so that higher transmit powers can be permitted or higher amplifier efficiencies enabled.

Many ways of achieving this goal have been proposed and investigated. Perhaps the most obvious is digital hard limiting of the signal where the modulation is generated. This is extremely crude and is effectively the same as subjecting the signal to a controlled nonlinearity. However it has been shown to be quite effective at reducing the magnitude of the problem [8-10].

Another way of tackling the problem is by coding the data such that the multiple modulated carriers are prevented from ever adding constructively. This was first proposed in [11] but no general means of performing the coding was identified. Suitable codes were identified and the potential gains explored in [12]. These two papers received a significant amount of attention in that many investigators attempted to solve the problem, for example see [13-16]. It was soon recognized that this technique was only really useful if no additional redundancy was introduced into the transmission by the use of this coding or in other words it would be advantageous if the same codes could be used for error control and envelope limitation. A method of manipulating standard FEC block codes to provide the additional benefit of envelope limitation with no additional redundancy was introduced in [17]. Whilst this was an acceptable engineering solution to the problem the envelope fluctuations achieved were still not ideal and there was no way of predicting what degree of envelope limitation would be achieved for a particular type of code. Finally, a more ideal solution to the problem was reported by Davis and Jedwab in [18] and presented in full in [19]. They exhibited a connection between Golay Complementary sequences and certain cosets of a generalisation of the classical Reed-Muller code. This gave a set of codes which had predictable and guaranteed error control and envelope limitation properties. Admittedly these codes might not have optimal error correction capability when compared with the standard alternatives but a reduction in coding gain could quite easily be outweighed by a greater reduction in envelope fluctuation. Ultimately this would result in improved system performance in terms of greater range or a reduced BER for the same transmit power limit or battery power limit. The aim of this paper is to present in detail the associated encoding and decoding procedures for these new coding techniques, and demonstrate through experimental and simulation results the achievable error rate performance over typical propagation channels, and also, the significant reduction in adjacent channel interference (ACI). It is only by quantifying both of these aspects of system performance that a realistic assessment of the benefit of these new coding techniques can be made. This enables a trade-off to be made between coding gain and amplifier input back-off, thus for a given set of hardware design constraints an optimal system design can be achieved.

Throughout the paper we use topical system design examples, typical propagation channel parameters and realistic amplifier characteristics to highlight the significance of the results. The structure of the paper is as follows. In Section 2, the background material is presented and the relationship between the aperiodic autocorrelation properties of the codewords and the power distribution of the OFDM signal is briefly discussed. Using a set of specific example codes, Section 3 details the relationship between Golay complementary sequences

and Reed-Muller codes, providing a framework which allows straightforward encoding. A maximum likelihood decoding algorithm is described in Section 4 and a specific example is used to illustrate the process. Section 5 presents the ACI performance, and Section 6 assesses the performance of the decoder for a number of realistic channel conditions. The paper is concluded in Section 7.

2 Background

The sampled complex envelope of an OFDM signal is given by

$$y_s(k) = \sum_{n=0}^{N-1} s_n W^{-nk} \quad , \quad k = 0,1,\ldots N-1 \tag{1}$$

where s_n is a complex symbol in the sequence $\mathbf{s} = [s_0, s_1, \ldots, s_{N-1}]$, N is the number of sub-channels, and $W = \exp(-j2\pi / N)$. The symbol s_n is taken from an alphabet of size $l = 2^p$, where p is the number of bits per symbol giving l^N distinct sequences. The instantaneous envelope power of the signal is the real valued function $P_s(k) = |y_s(k)|^2$, which is given by

$$P_s(k) = \sum_{m,n} s_m s_n^* W^{-mk} \left(W^{-nk}\right)^* \tag{2}$$

It is straightforward to show that the envelope power $P_s(k)$ is given by

$$P_s(k) = N + 2\,\mathrm{Re}\left\{\sum_{u=1}^{N-1} C_s(u) W^{-uk}\right\} \tag{3}$$

where $C_s(u)$ is the aperiodic autocorrelation of sequence $\mathbf{s}$ at displacement u, which is given by

$$C_s(u) = \sum_{m} s_m s_{m+u}^* \tag{4}$$

and the summation in (4) is over the integer values for which both m and $m+u$ lie within the range $0,1,\ldots,N-1$. From (3), we define the *peak envelope power* (*PEP*) as the supremum over a symbol period of $P_s(k)$. Similarly, the mean envelope power of any sequence is N, and we define the *peak-to-mean envelope power ratio* (*PMEPR*) of a sequence, $\mathbf{s}$, to be the ratio of PEP / N. Generally, *PMEPR* is expressed as $10\log_{10}(PEP / N), dB$.

If $\mathbf{s}=[1,1,\ldots,1]$ then the *PEP* of $P_s(k)$ is $N+2\sum_{u=1}^{N-1}(N-u)=N^2$. Therefore, the *PMEPR* of an uncoded OFDM signal is *N*. This result also applies to conventional linear block codes and convolutional codes. However, as reported in [20], by restricting the set of allowed sequences to be Golay complementary sequences we can reduce the *PMEPR* from its maximum value of *N* to at most 2: if sequences **a** and **b** are a Golay complementary pair, then by definition $C_a(u)+C_b(u)=0$ for each $u\neq 0$. Then from (2), $P_a(k)+P_b(k)=2N$ and since $P_b(k)=|y_b(k)|^2\geq 0$ we deduce that $P_a(k)\leq 2N$.

3 Encoding

In [19] a general framework for selecting OFDM codewords with good error-correcting properties and tightly bounded PMEPR is presented. In this paper we wish to illustrate in detail the associated encoding and decoding procedure and to demonstrate the achievable performance in terms of both channel time dispersion and ACI. For our purposes, it is sufficient to consider certain examples of quaternary coding with 16 subcarriers. In this way the practical significance can be emphasized as well as its practical implementation. Similar procedures and results can be obtained for other parameter and modulation choices described in [19].

Let $RM_4(1,4)$ be the linear code over $\mathbb{Z}_4$ with generator matrix

$$\mathbf{G}=\begin{bmatrix}1&1&1&1&1&1&1&1&1&1&1&1&1&1&1&1\\0&0&0&0&0&0&0&0&1&1&1&1&1&1&1&1\\0&0&0&0&1&1&1&1&0&0&0&0&1&1&1&1\\0&0&1&1&0&0&1&1&0&0&1&1&0&0&1&1\\0&1&0&1&0&1&0&1&0&1&0&1&0&1&0&1\end{bmatrix}\begin{matrix}1\\\mathbf{x}_1\\\mathbf{x}_2\\\mathbf{x}_3\\\mathbf{x}_4\end{matrix}$$

where the rows of the generator matrix are labelled $1,\mathbf{x}_1,\mathbf{x}_2,\mathbf{x}_3,\mathbf{x}_4$, as shown, and the codewords are all the modulo 4 linear combinations, for example $1\mathbf{x}_1+0\mathbf{x}_2+3\mathbf{x}_3+1\mathbf{x}_4+2.1=(1320021313200213)$. This quaternary code contains 4^5 codewords and is a natural generalisation of the familiar binary first-order Reed-Muller code $RM(1,4)$. We represent the componentwise product of the rows $\mathbf{x}_i$ and $\mathbf{x}_j$ by $\mathbf{x}_i\mathbf{x}_j$ in the usual way.

Let π be any permutation of the symbols $\{1,2,3,4\}$, let c, c_1, c_2, c_3, c_4 be any coefficients in $\mathbb{Z}_4$, and consider the quaternary codeword

$$[a_1, a_2, \ldots, a_{16}] = 2\left(\mathbf{x}_{\pi(1)}\mathbf{x}_{\pi(2)} + \mathbf{x}_{\pi(2)}\mathbf{x}_{\pi(3)} + \mathbf{x}_{\pi(3)}\mathbf{x}_{\pi(4)}\right) + c_1\mathbf{x}_1 + c_2\mathbf{x}_2 + c_3\mathbf{x}_3 + c_4\mathbf{x}_4 + c\cdot 1 \quad (5)$$

We know from Corollary 2.4 of [19] that the associated complex sequence

$$\mathbf{s} = \left[j^{a_1}, j^{a_2}, \cdots, j^{a_N}\right] \quad (6)$$

is a member of a quaternary Golay complementary pair, which by Section 2 has PMEPR at most 3dB. This complex sequence, rather than the quaternary codeword representation, is used as the input to the IDFT modulator of an OFDM system.

By taking all permutations π giving distinct coset representatives $2\left(\mathbf{x}_{\pi(1)}\mathbf{x}_{\pi(2)} + \mathbf{x}_{\pi(2)}\mathbf{x}_{\pi(3)} + \mathbf{x}_{\pi(3)}\mathbf{x}_{\pi(4)}\right)$ we can in this way identify 12 cosets of $RM_4(1,4)$ within the second-order quaternary Reed-Muller code $ZRM(2,4)$ (as introduced in [21]), each associated with 4^5 quaternary Golay sequences. Specifically, the 12 coset representatives are given by:

$\pi(1)$	$\pi(2)$	$\pi(3)$	$\pi(4)$	$2\left(\mathbf{x}_{\pi(1)}\mathbf{x}_{\pi(2)} + \mathbf{x}_{\pi(2)}\mathbf{x}_{\pi(3)} + \mathbf{x}_{\pi(3)}\mathbf{x}_{\pi(4)}\right)$
1	2	3	4	$2\left(\mathbf{x}_1\mathbf{x}_2 + \mathbf{x}_2\mathbf{x}_3 + \mathbf{x}_3\mathbf{x}_4\right) = (0002002000022202)$
1	2	4	3	$2\left(\mathbf{x}_1\mathbf{x}_2 + \mathbf{x}_2\mathbf{x}_4 + \mathbf{x}_3\mathbf{x}_4\right) = (0002020000022022)^*$
1	3	2	4	$2\left(\mathbf{x}_1\mathbf{x}_3 + \mathbf{x}_2\mathbf{x}_3 + \mathbf{x}_2\mathbf{x}_4\right) = (0000022000220202)^*$
1	3	4	2	$2\left(\mathbf{x}_1\mathbf{x}_3 + \mathbf{x}_3\mathbf{x}_4 + \mathbf{x}_2\mathbf{x}_4\right) = (0002020000200222)$
1	4	2	3	$2\left(\mathbf{x}_1\mathbf{x}_4 + \mathbf{x}_2\mathbf{x}_4 + \mathbf{x}_2\mathbf{x}_3\right) = (0000022002020022)$
1	4	3	2	$2\left(\mathbf{x}_1\mathbf{x}_4 + \mathbf{x}_3\mathbf{x}_4 + \mathbf{x}_2\mathbf{x}_3\right) = (0002002002000222)^*$
2	1	3	4	$2\left(\mathbf{x}_1\mathbf{x}_2 + \mathbf{x}_1\mathbf{x}_3 + \mathbf{x}_3\mathbf{x}_4\right) = (0002000200202202)^*$
2	1	4	3	$2\left(\mathbf{x}_1\mathbf{x}_2 + \mathbf{x}_1\mathbf{x}_4 + \mathbf{x}_3\mathbf{x}_4\right) = (0002000202002022)$
2	3	1	4	$2\left(\mathbf{x}_2\mathbf{x}_3 + \mathbf{x}_1\mathbf{x}_3 + \mathbf{x}_1\mathbf{x}_4\right) = (0000002202200202)$
2	4	1	3	$2\left(\mathbf{x}_2\mathbf{x}_4 + \mathbf{x}_1\mathbf{x}_4 + \mathbf{x}_1\mathbf{x}_4\right) = (0000020202200022)^*$
3	1	2	4	$2\left(\mathbf{x}_1\mathbf{x}_3 + \mathbf{x}_1\mathbf{x}_2 + \mathbf{x}_2\mathbf{x}_4\right) = (0000020200222002)$
3	2	1	4	$2\left(\mathbf{x}_2\mathbf{x}_3 + \mathbf{x}_1\mathbf{x}_2 + \mathbf{x}_1\mathbf{x}_4\right) = (0000002202022002)^*$

For convenience, we use eight of these coset representatives, giving an encoding method which map 13 information bits to 16 quaternary symbols. Three information bits select one of the eight coset representatives, the remaining ten information bits are converted to five quaternary information symbols c, c_1, c_2, c_3, c_4 and the codeword is then calculated from (5). As usual in QPSK systems [21], the conversion of pairs of information bits to quaternary symbols is carried out using the inverse of the Gray map, ϕ^{-1} where $\phi : \nu \mapsto \left(\beta(\nu), \gamma(\nu)\right)$ from $\mathbb{Z}_4$ to $\mathbb{Z}_2^2$ is given by

ν	$\beta(\nu)$	$\gamma(\nu)$
0	0	0
1	0	1
2	1	1
3	1	0

The maximum PMEPR of the codewords in this scheme is 3.0dB, whereas the maximum PMEPR in an uncoded scheme would be 12.0dB. We can modify this scheme, increasing the minimum Hamming distance in exchange for reduced code rate while maintaining the same maximum PMEPR, by using fewer than eight coset representatives [19]. In particular we can choose any four of the six coset representatives marked * above, or just a single coset representative, to give two additional coding options. The three options described have the following properties:

Option	**Minimum Hamming Distance**	**Minimum Lee Distance**	**# information bits per codeword**	**Code rate**
#1	8	8	10	0.31
#2	6	8	12	0.38
#3	4	8	13	0.41

Table 1: Quaternary coding options with 16 carriers and PMEPR at most 3.0dB

It is also possible to increase the code rate at the expense of a larger PMEPR by using more than eight cosets of $RM_4(1,4)$ in $ZRM(2,4)$, as described in [19]. The codewords of these more general coding schemes are not necessarily associated with Golay sequences.

4 Decoding

Suppose we use the quaternary coding scheme described above, compromising a union of R cosets of $RM_4(1,4)$ in $ZRM_4(2,4)$ with coset representatives $\{\mathbf{z}_1,\ldots\mathbf{z}_R\}$. We now give a maximum likelihood decoder for this code. The idea behind the decoder is to represent the linear code $RM_4(1,4)$ itself as the union of 16 cosets of $ZRM_4(1,4)$ having coset representatives $\{\mathbf{y}_1,\ldots,\mathbf{y}_{16}\}$, where $ZRM_4(1,4)$ is the linear code generated by the rows $1,2\mathbf{x}_1,2\mathbf{x}_2,2\mathbf{x}_3,2\mathbf{x}_4$. Now we know from [21] (where $ZRM_4(1,4)$ is denoted $ZRM(1,4)$) that the image under the Gray map ϕ of $ZRM_4(1,4)$ is the binary code $RM(1,5)$. This mapping is carried out by extending the Gray map given above to a map from $\mathbb{Z}_4^N$ to $\mathbb{Z}_2^{2N}$, taking $\phi(v_1,v_2,\ldots,v_N)$ to be

$$(\beta(v_1),\beta(v_2),\ldots,\beta(v_N),\gamma(v_1),\gamma(v_2),\ldots,\gamma(v_N)) \text{ for } v_i\in\mathbb{Z}_4. \tag{7}$$

We also have the identity

$$\phi(\mathbf{a}+\mathbf{b})\equiv\phi(\mathbf{a})+\phi(\mathbf{b})+(f(\mathbf{a},\mathbf{b})\| f(\mathbf{a},\mathbf{b})) \text{ for } \mathbf{a},\mathbf{b}\in\mathbb{Z}_4^N \tag{8}$$

where $f(\mathbf{a},\mathbf{b})$ denotes the componentwise product of the componentwise reductions modulo 2 of $\mathbf{a}$ and $\mathbf{b}$, and $\|$ denotes concatenation of length N vectors. Using this identity and the fact that $\mathbf{z}$ is a codeword of the form $2(\mathbf{x}_{\pi(1)}\mathbf{x}_{\pi(2)}+\mathbf{x}_{\pi(2)}\mathbf{x}_{\pi(3)}+\mathbf{x}_{\pi(3)}\mathbf{x}_{\pi(4)})$ (so that $f(\mathbf{z},\mathbf{a})=\mathbf{0}$ for any vector $\mathbf{a}$), the modulo 2 reduction of a codeword of $ZRM_4(1,4)$ is a constant vector, and that the modulo 2 reduction of $\mathbf{y}$ is a codeword of $RM(1,4)$, it can be shown that the image under ϕ of the coset $\mathbf{z}+\mathbf{y}+ZRM(1,4)$ is the coset $\phi(\mathbf{z})+\phi(\mathbf{y})+RM(1,5)$.

This motivates the algorithm for decoding a received codeword $\mathbf{r}$. For each allowed value of $\mathbf{z}$ and for each 16 values of $\mathbf{y}$, calculate $\phi(\mathbf{z})+\phi(\mathbf{y})+\phi(\mathbf{r})$ (reducing componentwise modulo 2) and decode it as an element $U=u_1\mathbf{x}_1+u_2\mathbf{x}_2+u_3\mathbf{x}_3+u_4\mathbf{x}_4+u\cdot 1$ of $RM(1,5)$.

This decoding can be efficiently carried out by means of the fast Hadamard transform (FHT) (described in detail in [22]), identifying a transform sequence element of largest magnitude to determine the coefficients u, u_i and therefore U. The 16 values of $\mathbf{y}$ can be represented as $y_1\mathbf{x}_1 + y_2\mathbf{x}_2 + y_3\mathbf{x}_3 + y_4\mathbf{x}_4$ (reducing componentwise modulo 4), where each y_i is 0 or 1. Select values $\mathbf{z}$ and $\mathbf{y}$ for which the Hadamard transform sequence element of largest magnitude for these values is maximal. The information bits corresponding to the selected coset representative $\mathbf{z}$ can be recovered directly by reference to the encoding procedure. To recover the remaining information bits, calculate the element $\phi^{-1}\left(U + \phi\left(\mathbf{y}\right)\right)$ of $RM_4(1,4)$ from the selected values $\mathbf{y}$ and U and use Gaussian elimination over $\mathbb{Z}_4$ with respect to the generator matrix $\mathbf{G}$ to determine the corresponding row coefficients c, c_1, c_2, c_3, c_4. Then convert these information symbols to information bits, outputting $\phi(c), \phi(c_1), \phi(c_2), \phi(c_3), \phi(c_4)$.

Alternatively, the information symbols c, c_1, c_2, c_3, c_4 can be recovered directly from the selected binary coefficients u_1, u_2, u_3, u_4, u and the selected value of $\mathbf{y} = y_1\mathbf{x}_1 + y_2\mathbf{x}_2 + y_3\mathbf{x}_3 + y_4\mathbf{x}_4$ without calculating U and without performing Gaussian elimination. Careful calculation, making use of (8), shows that c, c_1, c_2, c_3, c_4 are related to u_1, u_2, u_3, u_4, u and $y_1 + y_2 + y_3 + y_4$ by:

$$c = 2u + u_1 \tag{9a}$$

$$c_i = \left(2u_{i+1} + y_i\left(1 + 2u_1\right)\right) \bmod 4 \quad \text{for } i = 1,2,3,4. \tag{9b}$$

An alternative and more efficient method of calculating the information symbols c, c_1, c_2, c_3, c_4 is to note their relationship with the column positions 0,1,2,4 and 8 of the generator matrix $\mathbf{G}$. Let $\mathbf{d} = \phi^{-1}\left(U + \phi\left(\mathbf{y}\right)\right)$ then from $\mathbf{G}$, we note that

$$c = d_0 \tag{10a}$$

$$c_i = \left(d_{2^{4-i}} - c\right) \bmod 4 \tag{10b}$$

Decoding Example

Suppose the coding scheme uses a single coset of $RM_4(1,4)$ having coset representative $\mathbf{z} = (0002000200202202)$. From Table 1, the minimum Lee distance of this coding scheme is 8, so all errors of Lee weight at most 3 can be corrected. Suppose we encode the ten information bits (0100100111). Then $(c, c_1, c_2, c_3, c_4) = (1,0,3,1,2)$ and so the encoded element of $RM_4(1,4)$ is $c_1\mathbf{x}_1 + c_2\mathbf{x}_2 + c_3\mathbf{x}_3 + c_4\mathbf{x}_4 + c \cdot 1 = (1320021313200213)$ and the transmitted quaternary codeword is $\mathbf{z} + (1320021313200213) = (1322021113002011)$. Suppose this codeword is received, with an error of Lee weight 3, as $\mathbf{r} = (1322021213002031)$. Then

$$\phi(\mathbf{z}) + \phi(\mathbf{r}) = (01100100011001111010011010100100)$$

We add this value to $\phi(\mathbf{y})$ for each of the 16 possible values of $\mathbf{y}$: for example for $(y_1, y_2, y_3, y_4) = (0,1,1,1)$ we get $\mathbf{y} = (0112122301121223)$ and so

$$\phi(\mathbf{z}) + \phi(\mathbf{r}) + \phi(\mathbf{y}) = (01110011011100001101100011011010)$$

Each such expression is decoded as an element of $RM(1,5)$ in the standard way [22]: It is firstly converted from 0/1 form to +1/-1 form and then result of multiplication by the Sylvester-Hadamard matrix of order 32 is obtained by means of the FHT. An element of largest magnitude in the resulting transform sequence is identified. The position of this element within the vector (numbering the positions from 0 to 31) is expressed in binary to give the values $(u_1, u_2, u_3, u_4, u_5)$ and the sign of this element determines u (positive gives $u = 0$, negative gives $u = 1$). For example, for $(y_1, y_2, y_3, y_4) = (0,1,1,1)$ the transform vector is

$$(-2,2,2,-2,-14,14,-2,2,-2,2,2,-2,2,-2,-2,2,2,6,14,10,-2,-6,2,6,-6,-2,6,2,6,2,-6,-2)$$

and so -14 is an element of largest magnitude, occurring in position 4.

The complete set of results for all 16 values of **y** is:

$(y_1\ y_2\ y_3\ y_4)$	Transform sequence element of largest magnitude	Position number of this element within transform sequence
0000	18	3
0001	14	19
0010	18	19
0011	14	1
0100	18	19
0101	14	7
0110	26	19
0111	-14	4
1000	14	3
1001	10	2
1010	14	1
1011	10	1
1100	14	7
1101	10	7
1110	-14	13
1111	18	18

Table 2: Summary of FHT results for the 16 values of **y**

The entry of the maximum absolute value in Table 2 is +26 and is attained for $(y_1\ y_2\ y_3\ y_4) = (0110)$. This value occurs in position $19 = (10011)_2$ in the transform vector corresponding to this choice of **y**. Therefore we select $\mathbf{y} = y_2 + y_3 = (0011112200111122)$ and

$$U = u_1 + u_4 + u_5 = (01100110011001101001100110011001)$$

and calculate

$$\phi^{-1}\left(U + \phi\left(\mathbf{y}\right)\right) = (1320021313200213)$$

which is the original encoded element of $RM_4(1,4)$ with the errors due to transmission corrected. Using (9a),(9b) or (10a),(10b) we can directly determine the row coefficients c, c_1, c_2, c_3, c_4.

The quaternary maximum likelihood decoding procedure illustrated here for codewords of length 16 extends in a straightforward manner to general length 2^m, but not to general 2^p-phase decoding. If such a decoder is required, Algorithm 5.3 in [19] is suitable and highly efficient (though not maximum likelihood). In [30], Grant and van Nee also describe a soft decision maximum likelihood decoding algorithm for *q-ary* codes. However, this algorithm works in the complex domain and as such requires complex arithmetic operations, while the decoding algorithm described here, requires only real arithmetic.. The reader is referred to [31] for a comparison of the different decoding algorithms and their associated complexity.

5 Adjacent Channel Interference Performance

The purpose of this section is to demonstrate through experimental and simulated results the value of such codes in terms of ACI. We compare the ACI performance of an uncoded and coded signal for different levels of amplifier input back-off (IBO). Note, the uncoded system also corresponds to a coded system that exhibits the same PMEPR, e.g. convolutionally coded system.

For simulation purposes, we model the nonlinearity of the transmit amplifier chain by fitting a third-order polynomial to the AM-AM and AM-PM characteristics. The resulting output from the nonlinearity in complex envelope form is given by

$$y_A(t) = f_{AM}\left[|y(t)|\right]\exp\left(j\left(\arg(y(t)) + f_{PM}\left[|y(t)|\right]\right)\right) \tag{11}$$

where

$$f_{AM}\left[|y(t)|\right] = \begin{cases} G_{11}|y(t)| + G_{13}|y(t)|^3 & 0 \le |y(t)| < y_{i,sat} \\ V_{sat} & otherwise \end{cases} \tag{12}$$

$$f_{PM}\left[|y(t)|\right] = G_{21}|y(t)| + G_{23}|y(t)|^3 \tag{13}$$

The AM-PM function, f_{PM}, has units of *rads* and the AM-AM function, f_{AM}, produces a constant output voltage, V_{sat}, at input saturation, $y_{i,sat}$, and input levels beyond $y_{i,sat}$. The

nonlinearity used in the experiments is a complete 5GHz transmit chain, which consists of a pre-driver amplifier, a driver amplifier and final stage amplifier all biased in class A mode. The measured AM-AM and AM-PM characteristics are shown in Fig.1a and Fig.1b respectively. The output 1dB compression point of the line-up was measured as +22.5dBm for an input power of approximately -10dBm. This gives:

$$G_{11} = 47,\ G_{13} = -46\times 10^{3},\ G_{21} = -8,\ G_{23} = 150,$$

where $y_{i,sat} = 0.0183$ giving $V_{sat} = 0.5782$. Using these values, the third order curve fit for the AM-AM and AM-PM is also plotted in Fig.1a and Fig1b for comparison. Note, the constant phase offset produced by the AM-PM characteristic is -1.07*rad*, this value is not included in (13) as its has no effect on the performance. However, it has been included in the diagram in order to show the similarity between the experimental and fitted curves.

The experimental set-up is the same as that reported in [23]. It consists of an OFDM modulator which generates 16 subcarriers with quaternary PSK modulation. The OFDM symbol period is 953.67*ns* and the guard period including raised cosine shaping is 476.8ns. The carrier frequency is fixed at 5.29725GHz and the modulation bandwidth is 17.825792MHz. The coded system uses a single coset of $RM_4(1,4)$, and the coset representative is given by $2\left(\mathbf{x}_1\mathbf{x}_2 + \mathbf{x}_2\mathbf{x}_3 + \mathbf{x}_3\mathbf{x}_4\right)$.

Fig.2 shows the measured power spectrum of the uncoded signal for 4dB and 11dB IBO, included in the diagram is the input to the transmit line-up from the up-converted modulated output. It is clear that little improvement has occurred from 4dB to 11dB IBO, and in fact, significant spectral spreading is still evident even at 11dB IBO. Fig.3 shows the measured power spectrum of the coded signal at 0dB and 4dB IBO. The coded signal at 0dB IBO still appears better than the uncoded at 11dB IBO. Moreover, at 4dB IBO the degree of spectral spreading from the coded signal is insignificant.

These results are illustrated further in Fig.4, which shows the measured and simulated ACI performance as a function of IBO for both the uncoded and coded signals (the simulated results are obtained using the nonlinear model with identical system parameters as the experimental set-up). At 40dBc ACI, it is evident from the experimental results that the coded signal has approximately 12dB IBO gain over the uncoded signal, whilst the simulated results show only approximately 4dB IBO gain for the coded signal. By comparing the

simulated and experimental curves of the coded signal we see a good correlation between the results, whereas the uncoded signal shows a large difference of approximately 6dB between simulated and experimental curves.

This discrepancy between simulated and experimental results arises from the dynamic nature of the OFDM signal. The excessive peak excursions in the envelope of the uncoded signal, which are impulse-like, create disturbances in the devices and bias circuitry of the transmit chain, which temporarily alter the AM-AM and AM-PM characteristics. The simple time invariant cubic model is derived from experimental data, which is obtained by applying a continuous wave signal, or to be more precise, an unmodulated carrier to the transmitter chain at various levels of amplitude. As such, it is not representative of the nonlinear dynamic behavior of the transmit chain, which occurs when subjected to an uncoded OFDM signal. As the PMEPR is reduced, such that it approaches the envelope of the continuous wave signal this discrepancy becomes less pronounced, as shown by (i) and (ii) of Fig.4. In view of this, we recommend against the use of this modeling method, as it yields optimistic results for the uncoded OFDM signal.

An alternative approach for simulating the ACI performance, is to use equivalent circuit models to represent the electrical elements in the transmit chain. However, this can become unmanageable, and can still be unrealistic, since accurately including the non-electrical effects, such as temperature variations, is extremely difficult. Therefore, we conclude, that currently experimentation can be the only *true* indication of ACI performance when the envelope of the signal exhibits impulse-like behavior.

Finally, it is sufficient to say that if an alternative code is preferred, then for a given ACI, the coding gain offered by that code, has to overcome the combined IBO and coding gain of the Reed-Muller codes presented in this paper, as well as the more general class of codes described in [19]. For further details on this subject matter, the reader is referred to [24].

6 Indoor Radio Channel Performance

In the investigation of the performance of an OFDM transmission scheme by simulation it is important to use a realistic channel model. Just simply simulating performance in an additive white Gaussian noise channel is insufficient as this neglects both the positive effect of exploitation of the frequency diversity by the coding and the negative effect that the dispersion has on performance. As the introduction of such a channel model into the investigation introduces many new variables it becomes necessary to consider specific examples rather than general performance. In this paper we consider the example of an indoor wireless LAN system operating at 5GHz with a channel bandwidth of 20MHz. This is currently of interest as OFDM is being proposed for such systems as Wireless ATM which could be deployed in the HIPERLAN bands in Europe or the UNII bands in the US both at 5GHz.

For the carrier frequency and bandwidth stated above, the system design parameters are shown in Table 3. The OFDM symbol rate is 1Ms/s on every carrier. The gross bit rate for an uncoded system using 4PSK modulation is therefore $2 \times 1Mb/s \times N$. If $N = 16$, then the maximum uncoded data rate is 32Mb/s. Since, the guard period is $200ns$, the overall bandwidth of the transmitted signal is $N \times (1000ns - 200ns)^{-1}$ MHz, which is 20MHz for $N = 16$. Whilst we would not propose the use of uncoded OFDM, this comparison provides an indication of the achievable coding gain offered by the proposed coding scheme. It is left to the reader to make comparisons between this new coding scheme and more conventional schemes typically used with OFDM.

Parameters	# 1	# 2	# 3	Uncoded
Data Rate	9.92Mbits/s	12.16Mbits/s	13.12Mbits/s	32Mbits/s
Modulation	4PSK	4PSK	4PSK	4PSK
N	16	16	16	16
Code Rate	0.3125	0.375	0.40625	1
$[PMEPR]_{dB}$	3dB	3dB	3dB	12dB
Guard Period	200ns	200ns	200ns	200ns
Hamming Distance	8	6	4	1

Table 3 System Design parameters for the three coding options and the uncoded system

A. Channel Model

It is generally accepted that the indoor radio propagation channel is adequately modeled by a tapped delay line channel model with an exponential power delay profile with Rayleigh fading on the individual taps. This model is only valid when directional antennas are not used and where a line-of-sight is not guaranteed. The channel impulse response for a typical indoor radio channel can be modeled as [25]

$$h(t) = \sum_n a_n e^{-j\theta_n} e^{-\frac{\tau_n}{\sigma}} \delta(t - \tau_n) \tag{14}$$

where $h(t)$ is a sum of impulses with the *nth* impulse having a_n Rayleigh distributed amplitude, θ_n uniformly distributed phase, and τ_n delay. The RMS delay spread, σ, of the channel is given by

$$\sigma = \sqrt{\frac{\sum_n p_n \tau_n^2}{\sum_n p_n} - \left(\frac{\sum_n p_n \tau_n}{\sum_n p_n} \right)^2} \tag{15}$$

where p_n is the *nth* power component of $h(t)$.

B. Encoding and Modulation

Consider the block diagram shown in Fig.5. The data source produces symbols from an alphabet of size 2 {0 1} which have duration T secs. These symbols are formatted into a data vector which is segmented into 32 sub-blocks of length 10, 12, or 13 depending on choice of code. The first 10 bits of each sub-block is mapped from binary into quaternary under the gray map ϕ . The quaternary symbols are applied to the block encoder which produces a codeword from the $RM_4(1,4)$ generator matrix. Depending upon the code rate, the remaining bits are used to select the appropriate coset representative **z**.

The output of the encoder is a vector of 32 codewords which is subsequently applied to the packet assembler which appends the encoded vector to the end of a training sequence of 128 binary symbols. The training sequence is constructed from 8 OFDM symbols, whose PMEPR is bounded at most by 3.0dB. The output of the packet assembler is converted to complex symbols using the transformation given by (6), which results in 40 complex sequences each

of length 16, see Fig.(5). Each complex sequence is modulated by the IDFT onto 16 sub-channels producing one OFDM symbol. Each OFDM data symbol, is prefixed with a guard period which is equal to 0.25 of the encoded symbol period, and the oversampling rate is 4.Note, there is no guard period extension applied to the training sequence. The subsequent output is then converted into a serial stream for transmission.

C. Receiver

After transmission through the channel, the received signal is described by

$$r(t) = y_g(t) * h(t) + n(t) \tag{16}$$

where $y_g(t)$ is the OFDM signal with guard period extension, $h(t)$ is the composite channel impulse response (i.e. includes receive filtering, which is a 6th order butterworth filter with a 3dB double-sided bandwidth equal to $1/T$), and $n(t)$ is complex valued additive white Gaussian noise with zero mean and variance σ_n^2. If $r(t)$ is 4× oversampled and $t=lT$, then by normalising to T, (16) can be rewritten in the form

$$r_{l,q} = y_{g,l,q} * h_{l,q} + n_{l,q} \tag{17}$$

where $q=\{0...3\}$, $l = \{0,1,...M\}$, $M = 16\times 40 + b\times 32 + L - 1$, L is the effective ISI span of the channel impulse response, b is the guard period and $L,b \in \{0,1,2,3...\}$. The received signal is first applied to the synchronisation block, which uses a scheme similar to that described in [26,27]. We note that the receiver is coherent (i.e. performs phase equalization after DFT processing).

We describe the process of synchronisation with respect to Fig.5, which also includes the structure of the packet prior to modulation by the IDFT. The packet is partitioned into a synchronisation field and a data field. The synchronisation field consists of 8 sub-blocks, such that $\left[s_{i,0}...s_{i,15}\right], i = 0...7$ are Golay complementary sequences (for bounding the PMEPR), and we refer to the sequence of symbols for which $i=\{0,1\}$, $\forall n$ as the preamble. Synchronisation is performed in two stages:

i) Packet Synchronisation: Since the DFT requires an initial starting position, the first stage of synchronisation is concerned with performing temporal alignment with the strongest path in the channel impulse response. This is achieved by correlating the vector

$$\mathbf{r}_{\gamma,q} = \left[r_{0+\gamma,q} \cdots r_{31+\gamma,q}\right]^T,\ \gamma = \{0,1,\ldots L-1\} \tag{18}$$

with a filter which has T spaced tap weights defined by

$$\mathbf{w} = \begin{bmatrix} W^{-0\times0} & \cdots & W^{-0\times15} & 0 & \cdots & 0 \\ \vdots & \ddots & \vdots & \vdots & \ddots & \vdots \\ W^{-15\times0} & \cdots & W^{-15^2} & 0 & \cdots & 0 \\ 0 & \cdots & 0 & W^{-0\times0} & \cdots & W^{-0\times15} \\ \vdots & \ddots & \vdots & \vdots & \ddots & \vdots \\ 0 & \cdots & 0 & W^{-15\times0} & \cdots & W^{-15^2} \end{bmatrix} \begin{bmatrix} s_{0,0} \\ \vdots \\ s_{0,15} \\ s_{1,0} \\ \vdots \\ s_{1,15} \end{bmatrix} \tag{19}$$

which gives

$$h'_{\gamma,q} = \mathbf{w}^H \mathbf{r}_{\gamma,q} \tag{20}$$

where the first matrix in (19) represents the IDFT modulation process for two concatenated sequences, the second matrix is the preamble portion of the synchronisation field, H in (20) indicates the Hermitian transpose (i.e. conjugate transposition), $h'_{\gamma,q}$ in (20) is an approximated version of the channel impulse response. From the maximum correlation peak the start of packet is determined, which enables both synchronisation of the DFT (e.g. guard period removal) and decimation of the oversampled received signal. The decimation algorithm operates by taking every 4*th* sample with respect to the maximum correlation peak, thereby aligning the receiver with the strongest path in the channel impulse response. The preamble vector $\left[s_{0,0}\ldots s_{0,15}s_{1,0}\ldots s_{1,15}\right]^T$ which modulates the IDFT was selected on the basis of low correlation sidelobes around the correlation peak. The normalised modulus of the autocorrelation of $\mathbf{w}$ is shown in Fig.6, where the preamble is given by $\left[-11111-111-1-11-1111-1111-1-1-11-11-111-1111\right]$.

ii) Sub-channel Phase Synchronisation: The second stage of synchronisation determines the 16 sub-channel composite phase offsets at the output of the DFT, which is given by

$$\mathbf{h} = \mathbf{R}\mathbf{D}^T \tag{21}$$

where

$$\mathbf{h} = [h_{pk,0}, h_{pk,1}, \ldots h_{pk,N-1}]^T \tag{22}$$

$$\mathbf{R} = \begin{bmatrix} r''_{0,0} & \cdots & r''_{7,0} \\ \vdots & \ddots & \vdots \\ r''_{0,15} & \cdots & r''_{7,15} \end{bmatrix}, \mathbf{D} = \begin{bmatrix} s_{0,0} & \cdots & s_{7,0} \\ \vdots & \ddots & \vdots \\ s_{0,15} & \cdots & s_{7,15} \end{bmatrix}$$

and

$$\begin{bmatrix} r''_{i,0} \\ \vdots \\ r''_{i,15} \end{bmatrix} = \begin{bmatrix} W^{0\times 0} & \cdots & W^{0\times 15} \\ \vdots & \ddots & \vdots \\ W^{15\times 0} & \cdots & W^{15^2} \end{bmatrix} \begin{bmatrix} r'_{0+i16} \\ \vdots \\ r'_{15+i16} \end{bmatrix}, \; i = \{0 \ldots 7\} \tag{23}$$

The second matrix in (23) is the DFT matrix, , $h_{pk,n}$ is the correlation peak in the *nth* sub-channel, $[r'_{0+i16}, \ldots r'_{15+i16}]^T$ is the decimated version of the received signal after the first stage of synchronisation, and $[r''_{i,0}, \ldots r''_{i,15}]^T$ is the output of the DFT. The vector **h** is subsequently applied to the phase rotator for performing phase equalization during the reception of the data field. It should be noted that since indoor radio channels change at pedestrian speeds (<2m/s), it is assumed that the channel appears stationary for the duration of the packet. For a transmission frequency of 5GHz and a transmission rate < 25Mb/s this assumption holds when packet lengths are less than 20kbits [28]. Therefore, in the context of this paper, there is no requirement for tracking once both stages of synchronisation have been achieved.

After synchronisation, the receiver performs demodulation of the packet. The decimated serial received signal is converted into parallel format and the guard period is removed prior to demodulation by the DFT. The output of the DFT is described by the vector

$$\mathbf{r}''_i = [r''_{i,0}, r''_{i,1} \ldots r''_{i,15}]^T, \; i = \{8 \ldots 39\} \tag{24}$$

which is subsequently modified by the phase rotator giving $\mathbf{v}_i = \mathbf{r}''_i \mathbf{h}^*$, which corresponds to componentwise multiplication. The receiver makes a hard decision on a transmitted symbol, such that

$$\tilde{s}_{i,n} = \mathrm{sgn}\left(\mathrm{Re}[v_{i,n}]\right) + j\,\mathrm{sgn}\left(\mathrm{Im}[v_{i,n}]\right) \tag{25}$$

where sgn(.) is the signum function. The vector of complex symbols, $\tilde{\mathbf{s}}_i$, is mapped to $\mathbf{Z}_4$ and then $\mathbf{Z}_2$ using the distance preserving Gray map described in Section 3. The subsequent vector of binary symbols is then applied to the decoder.

7 Results

In order to validate the results we first compare the error rate performance of the simulation model against the theoretical curve in an AWGN channel, see Fig.7. The probability of error for the theoretical Gray mapped quaternary PSK OFDM signal is given by the familiar expression

$$P_e = \frac{1}{2} erfc \sqrt{\frac{E_b}{N_o}}$$

Comparing the theoretical curve against the uncoded shows a 1.5dB simulation loss at an error rate of 10^{-5}. It was found that this loss was attributed to the channel filtering, as the distribution of errors across the carriers exhibited a strong resemblance to the channel filter characteristic. Comparing the three coding options against the uncoded at an error rate of 10^{-5}, shows coding gains of approximately 1dB, 1.5dB and 1.9dB for options #1, #2, and #3 respectively.

The performance of the codes in a nonlinear channel have been excluded from the simulation results, as it was found that the degradation in error rate for practical values of ACI (>40dBc) was insignificant.

Next we consider the effect of σ on the performance of the uncoded and coded systems as a function of E_b / N_o. In the simulation 10^4 different channels were simulated for each value of σ, such that, the average power of the paths in the channel impulse response corresponded to an exponentially decaying profile. Fig.8, Fig.9 and Fig.10 show the error rate curves for three values of σ : 0ns, (which corresponds to a flat-fading channel), 25*ns*, and 50*ns*. These values were chosen based on propagation measurements taken at 5.2GHz, see [29] for details.

It is clear from Fig.8, that the uncoded OFDM signal out performs all of the coded options. This arises, since the number of errors per codeword produced by the flat-fading channel exceeds the number of correctable bits supported by the choice of code. Consequently, the maximum likelihood decoder may select a codeword which is significantly different from the original transmitted codeword. Therefore, unlike the uncoded signal, the maximum likelihood decoder can actually introduce additional bit errors into the coded signal.

As the channel becomes dispersive, as shown in Fig.9, the coding enables the OFDM signal to exploit the frequency diversity, whereas the uncoded signal suffers an irreducible error floor at high values of E_b/N_o. All coding options are capable of achieving BER$<10^{-3}$ for $E_b/N_o < 23dB$, furthermore, we note that option #1 (rate 0.31) offers the highest coding gain, whereas #2 and #3 are of comparable performance. As the RMS delay spread is increased from 25ns to 50*ns*, see Fig.10, option #1 still offers the highest coding gain, and in fact, performance is actually improved when compared to the 25*ns* curve of Fig.9. Note, the BER performance of options #2 and #3 are gradually beginning to degrade at values of $E_b/N_o > 26dB$. This is due to the intersymbol interference exceeding the guard period between OFDM symbols.

Although the data rate for the uncoded case is much greater than the coded, it is virtually unusable for the values of RMS delay spread considered in this evaluation. Based on results presented in [29], values of σ at 5GHz range between 4*ns* and 40*ns* in a residential or office cubicle environment. For this range of σ, the example coded systems are capable of providing usable error rates, whilst simultaneously reducing the linearity constraints on the system design. The results for the coding scheme compare favorably with conventional coding schemes typically used with OFDM for similar complexity [3].

8 Conclusion

We have presented coding schemes which enable the main criteria for a practical OFDM system to be simultaneously satisfied. An optimal code for a particular application of OFDM can be selected according to the set of system design constraints. We have also described a maximum likelihood decoding algorithm that operates on binary symbols using the FHT. Using a set of example codes and typical channel conditions, an end-to-end evaluation of the system performance improvement of these new coding techniques has been provided. We

have shown through the use of experimental and simulated results that these new codes provide superior ACI performance when compared to an uncoded OFDM system.

It is clear that the class of codes described in this paper may not offer the optimal performance in terms of coding gain, when compared to the more powerful convolutional codes. However, this has to be balanced against the benefits they offer in terms of envelope restriction and the associated reduction in IBO which translates to an overall improvement in amplifier efficiency.

Acknowledgments

We are grateful to both Jonathan Jedwab and Kenny Paterson for numerous helpful suggestions and discussions throughout this work..

References

[1] L.J.Cimini. Analysis and simulation of a digital mobile channel using orthogonal frequency division multiplexing. *IEEE Trans. Commun.*, **33**, no.7, pp.665-675, 1985.

[2] J.A.C.Bingham. Multicarrier modulation for data transmission: an idea whose time has come. *IEEE Commun. Mag.*, **28**, pp.5-14, 1990.

[3] M.Aldinger. Multicarrier COFDM scheme in high bit rate radio local area networks. *Proc. IEEE Symp. WCN, The Hague*, pp.969-973, Sept.1994.

[4] A.Alard and R.Lassalle. Principles of modulation and channel coding for digital broadcasting for mobile receiver. *EBU Review*, no.224, pp.3-25, 1987.

[5] F.Poegel, S.Zeisberg and A.Finger. Comparison of different coding schemes for high bit rate OFDM in a 60GHz environment. *Proc. IEEE ISSSTA, Mainz*, pp.122-125, 1996.

[6] H.Sari, G.Karam and I.Jeanclaude. Transmission techniques for digital terrestrial broadcasting,' *IEEE Commun. Mag.*,**33**, pp.100-109, 1995.

[7] E.McDonnell and T.A.Wilkinson. Comparison of computational complexity of adaptive equalization and OFDM for indoor wireless networks. *Proc. IEEE Symp. PIMRC, Taiwan*, pp.1088-1091 , 1996.

[8] R.O'Neil and L.Lopes. Performance of amplitude limited multitone signals. *Proc IEEE Conf. VTC, Stockholm*, pp.1675-1679, 1994.

[9] M.Schilpp, W.Saucer-Greff, W.Rupprecht And E.Bogenfeld. Influence of oscillator phase noise and clipping on OFDM for terrestrial broadcasting of digital HDTV. *Proc. IEEE ICC*, pp.1678-1682, 1995.

[10] L.Xiaodong and L.J.Cimini. Effects of clipping and filtering on the performance of OFDM. *Proc. IEEE Conf. VTC, Phoenix*, pp.1634-1638.

[11] A.E.Jones, T.A.Wilkinson and S.K.Barton. Block coding scheme for the reduction of peak to mean envelope power ratio of multicarrier transmission schemes. *IEE Electronics Letters*, **30**, no.25, pp2098-2099, 1994.

[12] T.A.Wilkinson and A.E.Jones. Minimisation of the peak to mean envelope power ratio of mulitcarrier transmission schemes by block coding. *Proc. IEEE VTC95, Chicago*, pp.825-829, 1995.

[13] D.Wulich. Reduction of peak to mean ratio of multicarrier modulation using cylic coding. *IEE Electronics Letters*, **32**, no.5, pp.432-433, 1996.

[14] D.J.Mestdagh and P.M.P.Spruyt. A method to reduce the probability of clipping in DMT-Based Transceivers. *IEEE Trans. Commun.*, **44**, no.10, pp.1234-1238. 1996.

[15] M.Friese. Multicarrier modulation with low peak to average power ratio. *IEE Electronics Letters*, **32**, no.8, pp.713-714, 1996.

[16] P.W.J.van Eetvelt, S.J.Shepherd and S.K.Barton. The distribution of peak factor in QPSK multi-carrier modulation,' *Inernational. Journal of Wireless Personal Communications, Kluwer*, **2**, no.1&2, pp87-96.

[17] A.E.Jones and T.A.Wilkinson, Combined coding for error control and increased robustness to system nonlinearities in OFDM. *Proc. IEEE VTC96, Atlanta*, pp.904-907, 1996.

[18] J.A.Davis and J.Jedwab. Peak-to-mean power control and error correction for OFDM transmission using Golay sequences and Reed-Muller codes. *IEE Electronics Letters*, **33**, no.4, pp.267-268, 1997.

[19] J.A.Davis and J.Jedwab. Peak-to-mean power control in OFDM, Golay complementary sequences and Reed-Muller codes. Technical Report HPL-97-158, Hewlett-Packard Labs., Bristol, Dec. 1997.

[20] B.M.Popovic. Synthesis of power efficient multitone signals with flat amplitude spectrum,' *IEEE Trans. Commun.*, **39**, no.7, pp1031-1033, 1991.

[21] A.R. Hammons, Jr., P.V. Kumar, A.R. Calderbank, N.J.A. Sloane, and P.Sole'. The Z_4-linearity of Kerdock, Preparata, Goethals, and related codes. *IEEE Trans. Inform. Theory*, **40**:301-319, 1994.

[22] F.J. MacWilliams and N.J.A. Sloane. *The Theory of Error-Correcting Codes*. North-Holland, Amsterdam, 1986.

[23] R.Castle and A.E.Jones. A 20Mb/s OFDM demonstrator: design, implementation and experimental results. *Proc. IEEE VTC98 Ottawa.* 1998.

[24] A.E.Jones T.A.Wilkinson and R.Castle. Adjacent channel interference performance of OFDM. ETSI BRAN Working Group 3 Temporary Document 79, Istanbul, Oct 1997.

[25] K.Pahlavan and A.H.Levesque. *Wireless infomation networks. Wiley*, 1st. Ed., 1995.

[26] L.J.Cimini, B.Daneshrad and N.R.Sollenberger. Clustered OFDM with transmitter diversity and coding. *Proc. GLOBECOM, London*, pp.703-707, 1996.

[27] T.Keller and L.Hanzo. Orthogonal frequency division multiplex synchronisation techniques for wireless local area networks. *Proc. IEEE Symp. PIMRC, Taiwan*, pp.963-967, 1996.

[28] J.Tellado-Mourelo, E.Kayata-Wesel and J.M.Cioffi. Adaptive DFE for GMSK in indoor radio channels. *IEEE JSAC,* **14**, no.3, pp.492-501, 1996.

[29] P.Hafezi, D.Wedge, M.A.Beach and M.Lawton. Propagation measurements of the 5.2GHz radio band in commercial and domestic environments. *Proc. IEEE Symp. PIMRC, Helsinki*, pp.509-513.1997.

[30] A.J. Grant and R.D.J. van Nee. Efficient maximum likelihood decoding of peak power limiting codes for OFDM. *preprint*, 1998.

[31] K.G. Paterson. Coding techniques for power controlled OFDM. *preprint*, 1998.

Figures

Fig.1a AM-AM characteristic, measured (solid line) and third-order fit (dashed).
Fig.1b AM-PM characteristic, measured (solid line) and third-order fit (dashed).
Fig.2 Spectrum plot of Uncoded OFDM, which also corresponds to a convolutionally encoded system, i.e. no envelope power control *PMEPR* = 12.0dB. i) 11dB IBO ii) 4dB IBO.
Fig.3 Spectrum Plot of Coded OFDM using a single coset of $RM_4(1,4)$, *PMEPR* = 3.0dB, i) 0dB IBO ii) 4dB IBO.
Fig.4 ACI performance for uncoded and coded OFDM:

(i) Coded Experimental
(ii) Coded Simulated
(iii) Uncoded Simulated
(iv) Uncoded Experimental

Fig.5 System block diagram for Reed-Muller encoded OFDM with Maximum Likelihood Decoding.
Fig.6 Absolute value of the normalised aperiodic autocorrelation of **w**.
Fig.7 Performance in an AWGN channel.
Fig.8 Performance in a flat-fading channel.
Fig.9 BER performance with an RMS delay spread of 25*ns*.
Fig.10 BER performance with an RMS delay spread of 50*ns*.

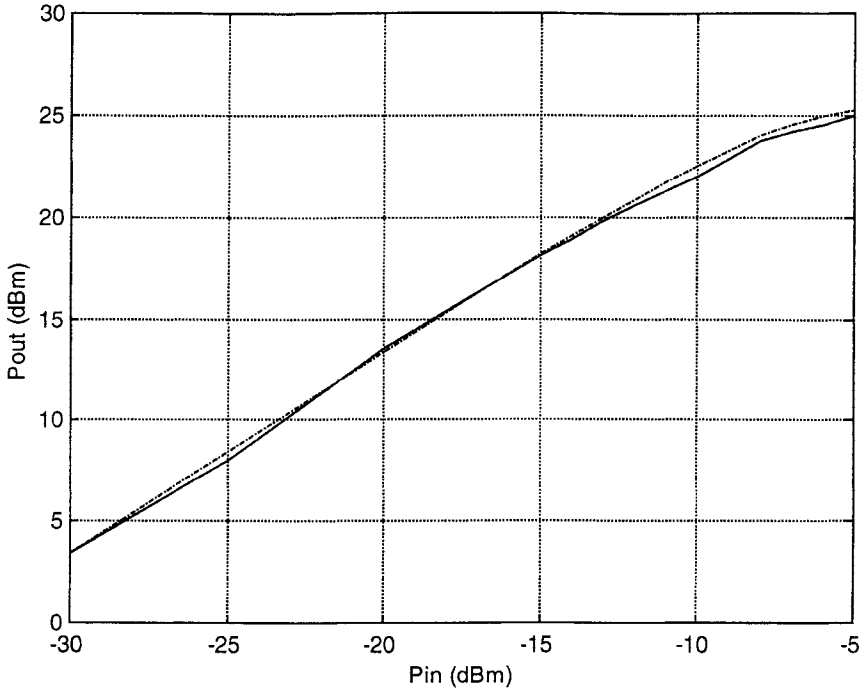

Fig.1a AM-AM characteristic, measured (solid line)
and third-order fit (dashed)

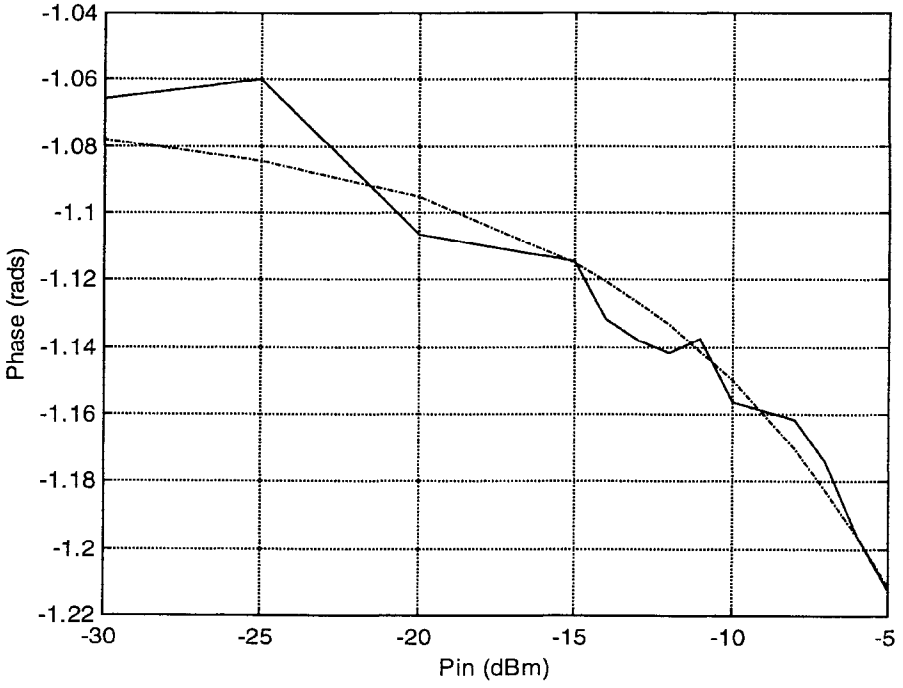

Fig.1b AM-PM characteristic, measured (solid line)
and third-order fit (dashed)

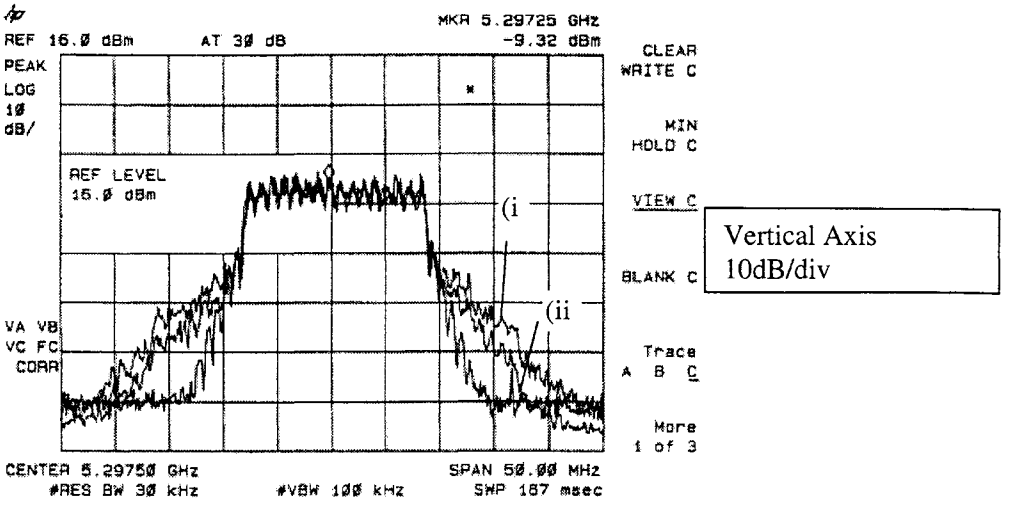

Fig.2 Spectrum plot of Uncoded OFDM, which also corresponds to a convolutionally encoded system, i.e. no envelope power control *PMEPR* = 12.0dB. i) 11dB IBO ii) 4dB IBO

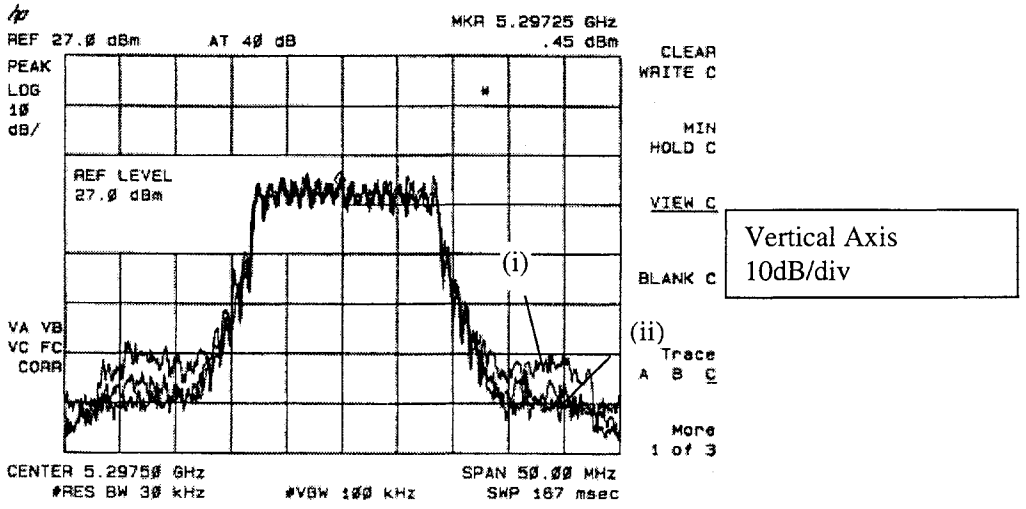

Fig.3 Spectrum Plot of Coded OFDM using a single coset of $RM_4(1,4)$, *PMEPR* = 3.0dB i) 0dB IBO ii) 4dB IBO

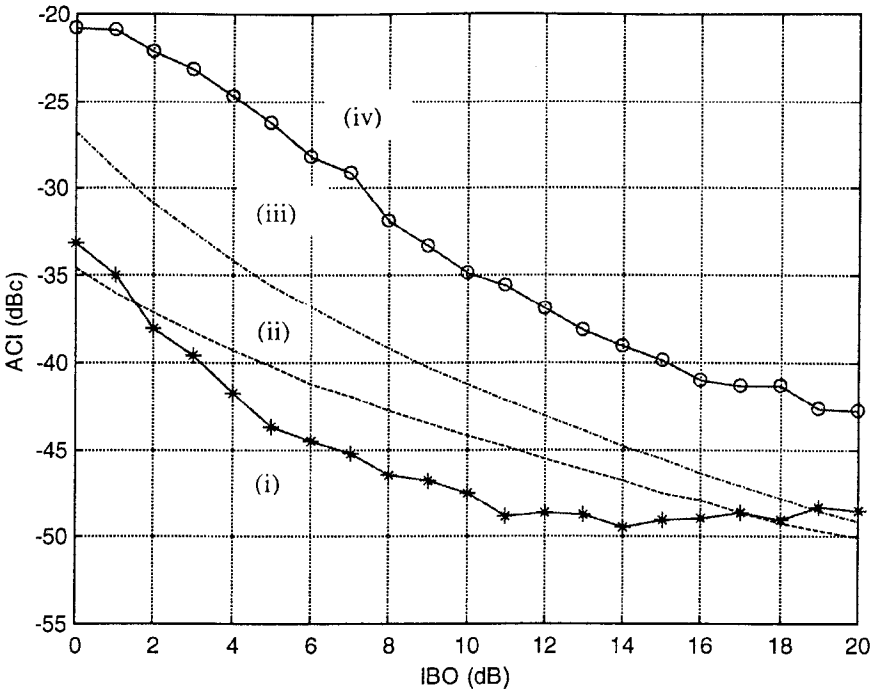

Fig.4 ACI performance for uncoded and coded OFDM:

(i) Coded Experimental
(ii) Coded Simulated
(iii) Uncoded Simulated
(iv) Uncoded Experimental

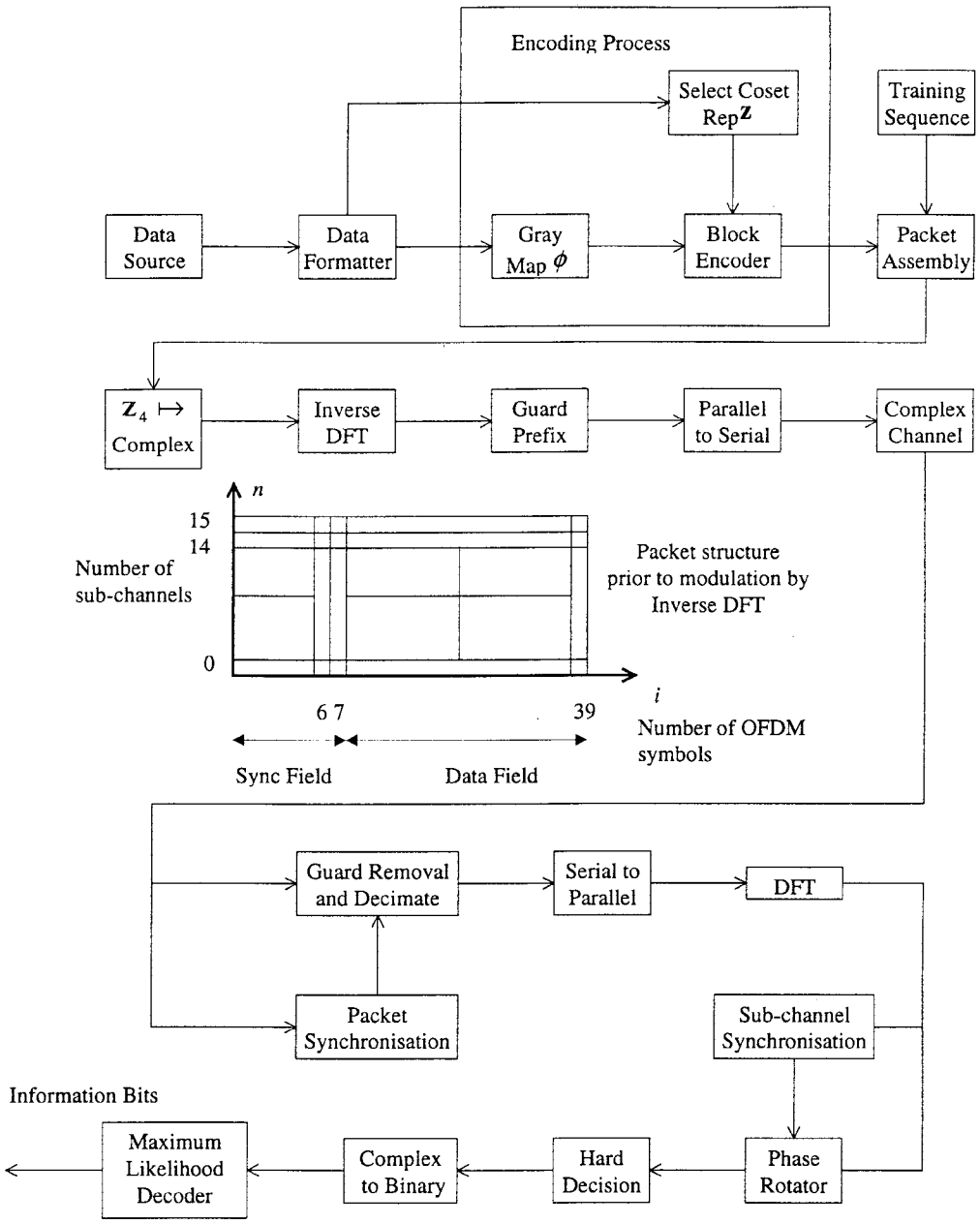

Fig.5 System block diagram for Reed-Muller encoded OFDM with Maximum Likelihood Decoding

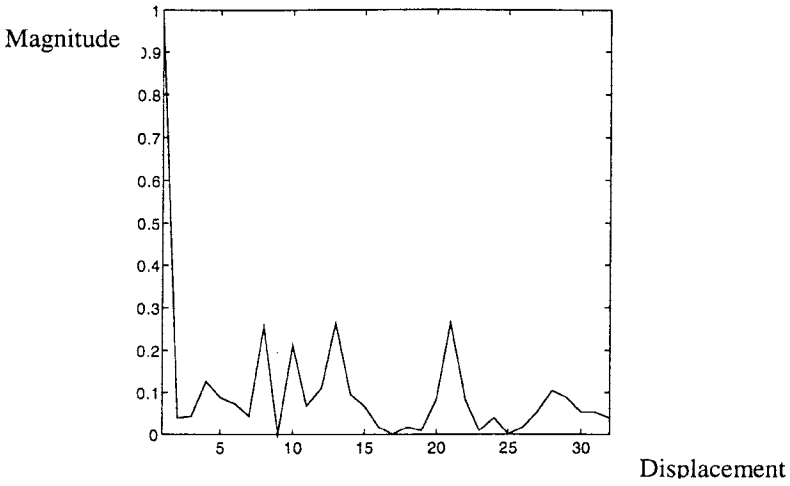

Fig.6 Absolute value of the normalised aperiodic autocorrelation of **w**.

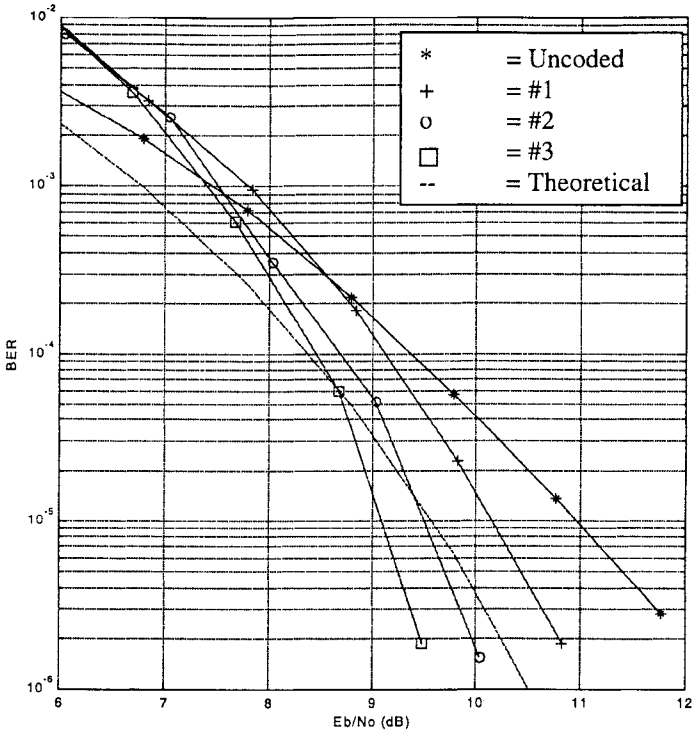

Fig.7 Performance in an AWGN channel

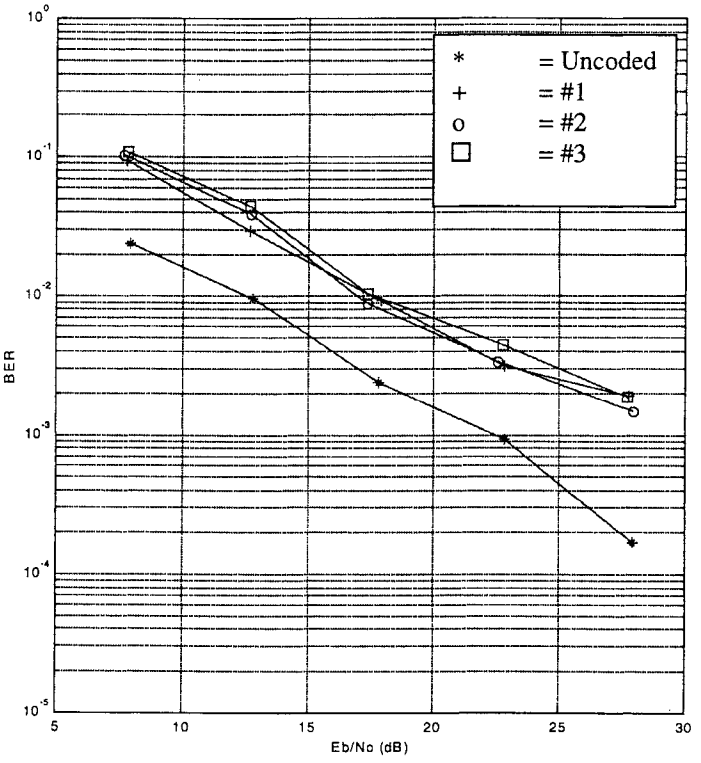

Fig.8 Performance in a flat-fading channel

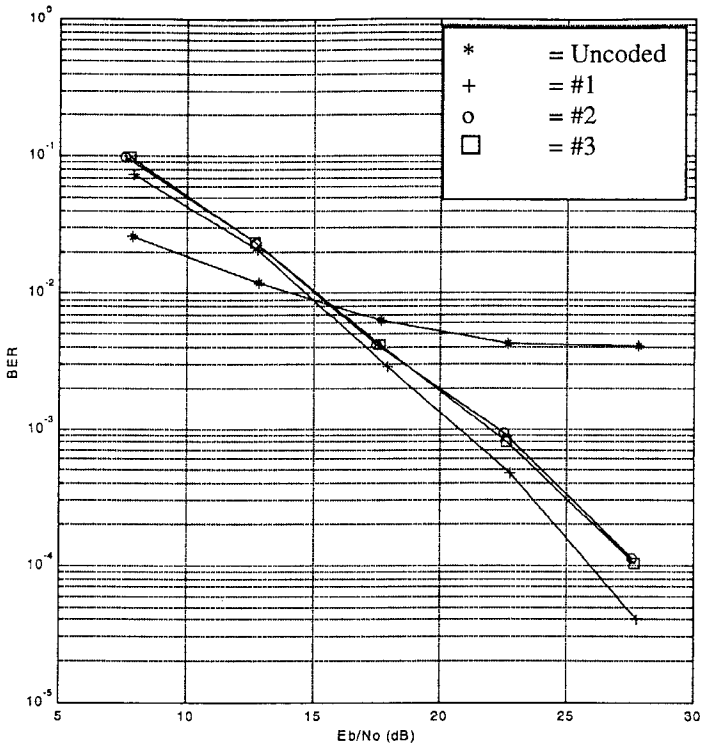

Fig.9 BER performance with an RMS delay spread of 25*ns*

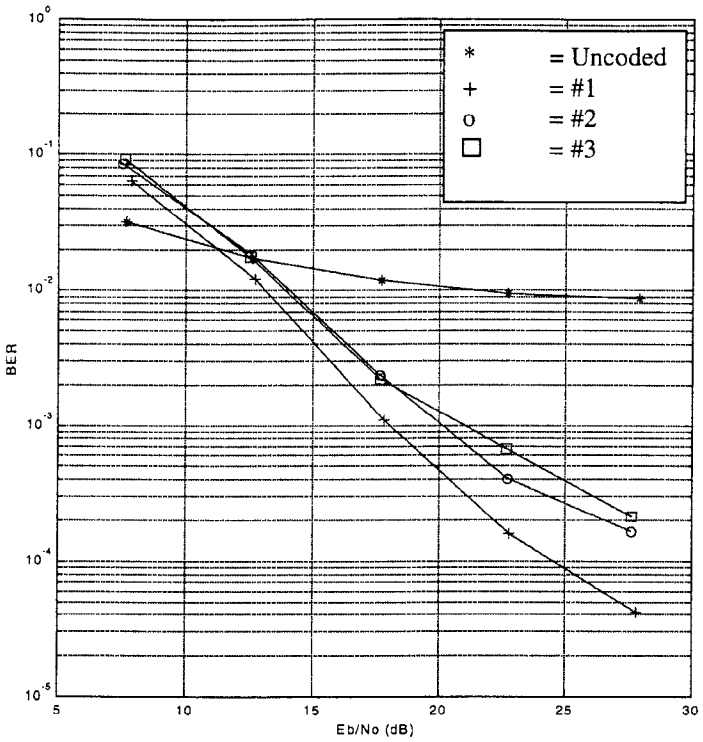

Fig.10 BER performance with an RMS delay spread of 50*ns*